

# MVTOP: Multi-View Transformer-based Object Pose-Estimation

Lukas Ranftl<sup>1,2</sup>Felix Brendel<sup>1</sup>Bertram Drost<sup>1</sup>Carsten Steger<sup>1,2</sup><sup>1</sup>MVTec Software GmbH, <sup>2</sup>Technical University of Munich

{lukas.ranftl; felix.brendel; bertram.drost; carsten.steger}@mvttec.com

## Abstract

We present MVTOP, a novel transformer-based method for multi-view rigid object pose estimation. Through an early fusion of the view-specific features, our method can resolve pose ambiguities that would be impossible to solve with a single view or with a post-processing of single-view poses. MVTOP models the multi-view geometry via lines of sight that emanate from the respective camera centers. While the method assumes the camera interior and relative orientations are known for a particular scene, they can vary for each inference. This makes the method versatile. The use of the lines of sight enables MVTOP to correctly predict the correct pose with the merged multi-view information. To show the model’s capabilities, we provide a synthetic data set that can only be solved with such holistic multi-view approaches since the poses in the dataset cannot be solved with just one view. Our method outperforms single-view and all existing multi-view approaches on our dataset and achieves competitive results on the YCB-V dataset. To the best of our knowledge, no holistic multi-view method exists that can resolve such pose ambiguities reliably. Our model is end-to-end trainable and does not require any additional data, e.g., depth.

## 1. Introduction

The six-degree-of-freedom (6-DoF) pose estimation task involves determining both the position  $(x, y, z)$  and the orientation (represented, e.g., by pitch, yaw, and roll) of objects. It is an extension of object detection, where only a bounding box with center coordinates  $(x, y)$  and size (width, height) is predicted. Estimation of the 6-DoF pose of objects remains crucial in tasks such as robotic manipulation [1–7], augmented reality [8–10], or industrial automation [11, 12].

There are methods that approach this problem from a rule-based perspective, but the leaderboards of common benchmarks have been topped by deep-learning-based methods for some time now [13, 14]. Usually, a backbone is used to extract image features. In indirect approaches,

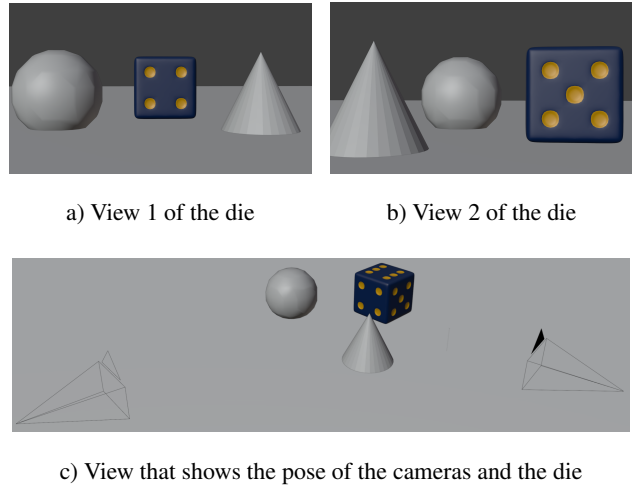


Figure 1. A die viewed from camera 1 (a), camera 2 (b), and from a larger distance with both cameras visible (c) (the cone and sphere are in the scene merely to aid in understanding the scene.) With the information of one view alone, the die’s pose cannot be determined. It can only be determined if the information of both views is considered.

the features are used to generate 2D–3D correspondences that are used by the PnP algorithm to determine the object pose. In contrast, direct approaches use the features to directly regress the pose. Many methods pass additional depth information as an additional channel (RGB-D) to improve the pose estimate along the  $z$ -axis. However, using additional depth maps is related to higher financial costs since depth cameras are usually more expensive than RGB cameras, and it can also introduce a higher computational burden. Instead, multiple RGB images of the same scene can be used to determine the object pose. Because multiple views introduce geometric consistency, the depth estimate can be improved without requiring a depth map. Furthermore, pose ambiguities where the pose of an object cannot be inferred from one view can be solved with the help of additional views, e.g., a cup where the handle is not visible in the first view.

In situations where the pose cannot be inferred from one view alone, an early fusion and processing of the view-specific features is essential. This can be visualized using a regular die (Figure 1). For each view of the die (Views 1 and 2), four possible poses are valid, i.e., four rotations around  $90^\circ$  along the current view axis. A correct pose estimation with either of these views is impossible. The correct die pose can be determined only by combining the information of both views, i.e., by knowing their relative camera poses. For the die, this pose ambiguity is discrete and limited to four possible poses. However, there are cases where the pose ambiguity is continuous (see Sec. 3). In the special case of the die, one can think of hand-crafted solutions where a multi-view pose estimation network could predict a set of poses (in this case four) for each view, and via a consistency check, the correct pose could be inferred; see, e.g., [15]. However, such approaches may not generalize well and also fail for objects where the set of poses that match an observation is not discrete but continuous. Additionally, occlusion can induce ambiguities that cannot be enumerated exhaustively in an offline pre-processing stage. Overall, resolving pose ambiguities in a post-processing phase in which only poses from single views are considered is inherently very difficult.

Our presented network can tackle such ambiguities in an end-to-end manner without the need for fine-tuning it to the objects or the camera setup. Especially in an industrial context, the acquisition of depth data can be associated with excessive costs, as multiple RGB cameras are usually cheaper than one 3D-sensor, which is why our approach only requires RGB data. Furthermore, our multi-view approach can process the input views in an arbitrary order because the network learns to handle ray information generated by the internal and relative orientations of the cameras. The attention mechanism [16] ensures an exchange of information between the different camera viewpoints and allows the handling of ambiguities as well as a better pose estimation in general.

Our main contributions are as follows:

- We provide the novel synthetic multi-view pose estimation dataset named MV-ball that contains images of an object with pose ambiguities that are only solvable by early incorporation of information from multiple views. The dataset is used to demonstrate the advantages of our proposed method MVTOP.
- For the first time, we introduce a novel multi-view pose estimation framework that fuses view-specific features in an early stage and is end-to-end trainable. By merging line-of-sight information and multi-view features and processing them using the attention mechanism, the network can build a strong and discriminative scene understanding. This allows the model to determine the correct pose for objects that are unsolvable for single-view meth-

ods.

- Our method outperforms existing methods on the MV-ball dataset, which we introduce to highlight the above-mentioned ambiguities of poses. On the YCB-V dataset, we achieve competitive results.
- Our model uses only RGB images and the interior and relative orientations of the cameras. It does not require additional depth information or 3D models for Inference. 3D models are only required for the generation of training data. Furthermore, the views/images can be fed to the model in an arbitrary order since it learns to handle the relative orientations of the camera to build up a spatial understanding of the 3D scene.

## 2. Related works

### 2.1. Object pose estimation

The field of object pose estimation can be divided in various ways. Within the following overview we focus on the learning based single- and multi-view approaches that are fine-tuned on one or multiple objects. Here, there are distinctions in terms of model architecture, input data, and post-processing.

Most of the existing direct methods apply a CNN from which the poses are regressed directly [17–19]. In [20], the network uses a differentiable PnP head to find the object poses.

Many indirect methods infer the pose by applying the PnP algorithm on 2D–3D correspondences [21–26]. In [27], an autoencoder is used together with an ICP module to predict the pose. In addition, there are approaches that use the 3D model to generate templates that are then matched with the objects in the image to find the poses [28, 29]. In [30], the network predicts bit masks from which the pose is determined using the PnP algorithm.

Recently, attention-based transformer architectures have been explored for pose estimation. In [31], the Detection Transformer DETR [32] is adapted to the task of estimating poses. Since this approach includes a symmetry-aware loss, the method needs 3D models of the objects. The method in [33] is based on Deformable DETR [34] and requires only one RGB image to predict the pose. No 3D models or additional information are necessary and the network is end-to-end trainable.

The research in the field of multi-view pose estimation is rather sparse. The methods in [35–37] are multi-view methods that require depth information. To our knowledge, so far there are only two methods that rely solely on RGB images [15, 38]. The network in [38] consists of several stages. The first stage generates pose candidates for each view separately. For this, any single-view pose estimator could be used. In the next stage, the candidates are matched across the views using a RANSAC-based method. The matches

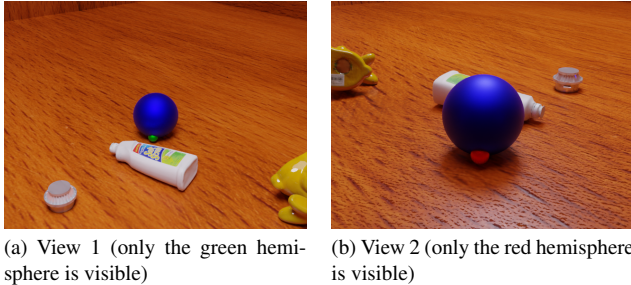


Figure 2. Example view pair of the MV-ball training split. View 2 differs by approximately  $180^\circ$  with respect to the axis pointing upwards from the floor

are used to build a graph that links consistent poses. In a final step, the poses are refined by minimizing a multi-view reprojection error. However, this approach cannot deal with pose ambiguities as described in Sec. 1 since the network does not fuse multi-view information before the pose prediction. In [15], the network produces a set of the top-K poses for each view. In a common reference frame, the pose hypotheses are compared and scored via a voting scheme. Therefore, ambiguities can be resolved using cross-view consistency, but only in discrete cases.

## 2.2. Object pose estimation datasets

Several datasets have been proposed for object pose estimation. Many of them are part of the well-known BOP Challenge [13, 14]. The most important ones are the core datasets of the main track, which have been part of the Challenge since 2019. The datasets within this track are Linemod-Occluded [39], T-LESS [40], ITODD [41], HomebrewedDB [42], YCB-V [19], IC-BIN [43], and TUD Light [44]. The test sets contain real RGB/monochrome (+depth) images and the train sets contain real and/or synthetic RGB/monochrome (+depth) images. The BOP-H3 track features the three datasets HOPE [45], HANDAL [46] and HOT3D [47]. These datasets focus on household objects and some include additional hand poses. Recently, an additional track (BOP-Industrial) was opened that focuses on industrial objects and also includes multiple views [14]. The datasets XYZ-IBD [48], IPD [49], and ITODD [41] were included in this track. Furthermore, the ROBI dataset [50] models a bin picking scenario, where each bin is filled with one of seven industrial objects. Although there are already many datasets, to the best of our knowledge, only HOT3D [47] contains an object (a Rubik’s cube) that is ambiguous from multiple views. However, the images in this dataset also contain objects that are not ambiguous. This motivated us to generate a dataset that covers exactly this gap.

## 3. MV-ball dataset

To evaluate the ability of a method to combine visual information from multiple views, we designed a dataset where single images can only result in ambiguous poses. To predict a correct pose, multiple views would have to be fused by necessity and therefore all single-view methods, as well as methods that naively fuse poses of single-view results, are expected to fail on this dataset. Existing datasets cannot highlight the nature of such ambiguous poses. In YCB-V [19], objects such as a mug are ambiguous if the handle is not visible. As soon as the handle is visible, the pose can be correctly determined. In theory, this makes such objects solvable with a single view. No existing dataset contains objects that are ambiguous from multiple views.

To allow for many ambiguous views, two hemispheres were extruded from a sphere at a relative angle of  $90^\circ$ , as can be seen in Fig. 2. With this object, all views that do not include both hemispheres are ambiguous since the position of the second extruded hemisphere can only be guessed. To generate a dataset of ambiguous views, blenderproc [51] was used to place objects in scenes and let them fall to the floor together with random distractor objects. To avoid a bias in the dataset, the two hemispheres were modeled with no mass, which means the hemisphere would not rotate towards the ground due to the influence of gravity. This means that the two hemispheres do not always point towards the ground plane but also point upwards in the world, and a larger range of poses is covered. The resulting scenes were used to find camera poses in which only one of the two hemispheres is visible by setting pixel thresholds of how many pixels per hemisphere must be visible. In our setup, we used the thresholds to create test sets of different difficulty — the easy test set with more than 300 pixels visibility and a hard test set with more than 10 pixels visibility, with a total image resolution of  $640 \times 480$  pixels. Our dataset consists of 112,042 images for training and 3853 or 3458 images for testing/evaluating with the easy or hard set, respectively. With multiple instances in one image, some of them might be solvable with one view, while others would not be solvable at all (if no hemisphere is visible). Therefore, every image in our dataset contains only one instance to ensure that the metric for such an image would be distinct.

## 4. MVTOP method

Our work is inspired by PoET [33] and the human pose estimation network in [52]. Both are based on Deformable-DETR [34]. In the predecessor DETR, features of the whole image are considered, whereas in Deformable-DETR, attention is established only between local features around specific reference points [32]. In [52], the poses of multiple people are predicted with information from multiple

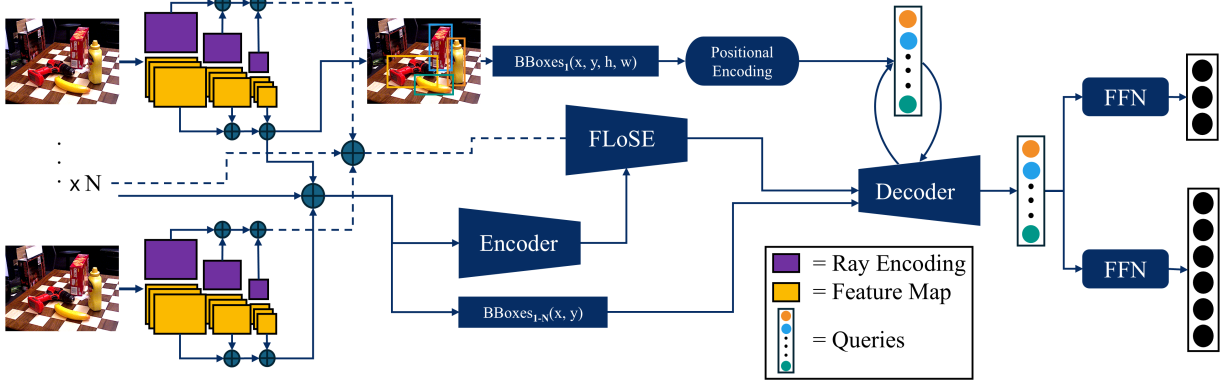


Figure 3. The MVTOP network. Our model takes  $N$  input images of different views. An object detector extracts multi-scale features (yellow) and predicts bounding box coordinates for each image. Additionally, the lines of sight for the feature maps are encoded (purple) using the interior and relative orientations of the cameras. By merging this line-of-sight information with the encoded multi-scale multi-view features, the decoder can produce a 3D aware update of the queries that were generated from the bounding box information of the first image. Finally, two separate heads predict rotation and translation for each query.

images. To improve generalization, the network uses so-called joint query embeddings, which encode person and joint information together. Furthermore, a module named projective attention is introduced, which takes local features around the 2D projections coming from 3D points. Thereby, the model fuses multi-view features. This is enriched with RayConv, which is a module that encodes camera ray directions into the feature vector.

Our network takes  $N$  input images and processes them via an off-the-shelf object detector to extract multi-scale features and bounding box information. Additionally, the multi-scale features are enriched with line-of-sight information that encodes both the interior and relative orientations of the cameras. The gathered information is processed by an attention-based encoder-decoder transformer. The output of the transformer is processed with a rotation head and a translation head. Our method is visualized in Fig. 3 and is described in detail in the following section.

#### 4.1. Network architecture

First, the  $N$  input images are passed to the object detector (OD). It processes each view separately and extracts multi-scale features, classes, and bounding-box information. The multi-scale features are fed into the attention-based encoder, which generates a suitable embedding for the decoder.

For every pixel in every feature map, the line of sight is calculated using the interior and relative orientations of the cameras. This information is merged with the encoded feature maps in a step which was introduced as RayConv in [52]. We adapted this operation and call it FLoSE (Feature Line-of-Sight Encoding) which is explained in more detail below. The spatially enriched and encoded feature maps are processed by the decoder.

In the Decoder, the first image serves as a reference image for which the pose prediction will be made. The center values of the bounding boxes of the first image are used to generate a set of object queries, which will be processed by the decoder. The center values of each bounding box of each object in each image are given as reference points to the decoder. These reference points are used within the projective attention module to sample features in the region around the found objects. By not extracting dense features but only features within the vicinity of the objects of interest, computational cost can be reduced. Furthermore, the gathered features are more discriminative.

Finally, the rotation and translation heads predict the pose components for each query for the first image. The translation and rotation heads are unchanged compared to the implementation of PoET [33].

The center values of the objects in each view allow only limited 3D scene understanding. To enrich the model with more spatial information, we adapt the RayConv operation of [52]. Our goal was to train a model that is capable of dealing with arbitrary camera setups and sequences of camera input. To do so, the lines of sight are calculated for the feature maps using the interior and relative orientations of the cameras. One possible parameterization consists of the origin and direction. This results in six values for each pixel. Other parameterizations are examined in Section Sec. 6. By randomly combining views in each iteration, the model learns to handle a new camera setup at inference. The feature vector generated by the encoder is concatenated with the encoded lines of sight and is then projected back to the encoding dimension using a linear layer. While the original RayConv operation only enriched the feature vector with the ray direction, our approach also encodes the ori-

gin. We call this operation FLoSE (Feature Line-of-Sight Encoding), which can be defined as follows:

$$\hat{\mathbf{F}}_v = \text{Concat}(\mathbf{F}_v, \mathbf{R}_v) \mathbf{W}^\top . \quad (1)$$

$\mathbf{F}_v \in \mathbb{R}^{*,d_{\text{model}}}$  are the encoded multi-scale features and  $\mathbf{R}_v \in \mathbb{R}^{*,6}$  are the parametrized lines of sight. After concatenation, they are transformed back to the embedding dimension with the learned weights  $\mathbf{W}^\top \in \mathbb{R}^{d_{\text{model}} \times (6+d_{\text{model}})}$ . The resulting spatially enriched feature vector  $\hat{\mathbf{F}}_v \in \mathbb{R}^{*,d_{\text{model}}}$  can then be used within the projective attention module to sample local features in the vicinity of the objects.

The model needs to sample features of the vector  $\hat{\mathbf{F}}_v$ . As described in Deformable-DETR [34], this can be done with so-called reference points. Within the projective attention module of [52], these points are generated by projecting 3D joint locations into the corresponding 2D image locations using the camera orientation parameters. We adapted this module to work within the setup of multi-view object pose estimation. The object detector already provides suitable reference points for each view, namely the center values of the bounding boxes of the objects. The features are then collected from  $K$  discrete sampling points away from the center  $\mathbf{c}$ . These sampling offsets are estimated by projecting the query feature  $\mathbf{q}$  and the spatially enriched feature  $\hat{\mathbf{F}}_v(\mathbf{c})$  with the learnable linear weight  $\mathbf{W}^p$ , i.e.,

$$\Delta \mathbf{c} = (\mathbf{q} + \hat{\mathbf{F}}_v(\mathbf{c})) \mathbf{W}^p . \quad (2)$$

At these sampling locations, the corresponding  $\hat{\mathbf{F}}_v$  are extracted and an attention weight  $\mathbf{a} = \text{Softmax}((\mathbf{q} + \hat{\mathbf{F}}_v(\mathbf{c})) \mathbf{W}^a)$  is applied linearly. This leads to the following definition for the projective attention:

$$\begin{aligned} \text{PAttention}(\mathbf{q}, \mathbf{p}, \{\hat{\mathbf{F}}_v, v = 1, \dots, V\}) \\ = \text{Concat}(\mathbf{f}_1, \mathbf{f}_2, \dots, \mathbf{f}_V) \mathbf{W}^p , \end{aligned} \quad (3)$$

where

$$\mathbf{f}_v = \sum_{k=1}^K \mathbf{a}(k) \cdot \hat{\mathbf{F}}_v(\mathbf{c} + \Delta \mathbf{c}(k)) \mathbf{W}^f . \quad (4)$$

Here,  $\mathbf{W}^p$  and  $\mathbf{W}^f$  are learnable linear weights. The projective attention is applied within each decoder layer, where the cross-attention can learn relationships between the different views.

The decoder outputs object queries, which are processed by the rotation and translation heads. Both heads are multi-layer perceptrons (MLPs) and remain unchanged with respect to the implementation in PoET [33]. This means that the translation head predicts the three translation values  $\mathbf{t}^p = (t_x^p, t_y^p, t_z^p)$  for the reference view. Consequently, the loss is determined as in PoET [33]:

$$L_t = \|\mathbf{t} - \tilde{\mathbf{t}}\|_2 . \quad (5)$$

The rotation head directly predicts a 6D rotation representation from which the  $3 \times 3$  rotation matrix can be recovered using the Gram-Schmidt orthogonalization by interpreting the 6 values as two vectors. The 6D representation ensures a stable training with the least number of values. This is described in detail in [53] where it was explained that such a 6D representation is favorable. The loss is calculated via the trace of the matrix product of prediction  $\tilde{\mathbf{R}}$  and ground truth  $\mathbf{R}$  rotation:

$$L_{\text{rot}} = \arccos \frac{1}{2} \left( \text{Tr}(\mathbf{R} \tilde{\mathbf{R}}^T) - 1 \right) . \quad (6)$$

Both losses are weighted with  $\lambda_t$  and  $\lambda_{\text{rot}}$  to obtain the total loss of

$$L = \lambda_{\text{rot}} L_{\text{rot}} + \lambda_t L_t . \quad (7)$$

In [33], two different approaches with respect to the number of classes are compared. In the class-specific case, the output dimensions of the translation and rotation head are  $3 \times n_{\text{cls}}$  and  $6 \times n_{\text{cls}}$ , respectively, while in the class-agnostic case, the dimensions are 3 and 6 for translation and rotation. Because [53] describes that the class-specific case yielded better results, we continued with this approach.

## 5. Experiments

In this section, the experiments we have conducted are explained. Of the existing multi-view methods, only the code of CosyPose [38] is publicly available. Therefore, it is the only multi-view method we could test on the MV-ball dataset. Furthermore, we evaluated PoET [33] on the MV-ball dataset since it is a SOTA pose estimation algorithm and served as a basis for our approach. For the YCB-V dataset additional approaches were compared with our approach.

### 5.1. Metric

To evaluate our model, we used the mean ADD-(S) error introduced by [54] and the rotation/translation error in [55] for the MV-ball dataset. The rotation error is of particular interest since it can better highlight the benefits of our multi-view approach if applied on the MV-ball dataset. On the YCB-V dataset, we use the AUC of the ADD-S metric since this is a commonly used metric for this dataset.

### 5.2. Datasets

As mentioned in Sec. 3, we developed our own dataset MV-ball to prove the true multi-view nature of our approach. We investigated the influence of the visibility of the hemispheres with the two different test sets.

Furthermore, we evaluated our model on the YCB-V dataset [19], which is a well established pose estimation dataset and also part of the BOP Challenge [13, 14] (see Sec. 2). Our model requires the interior and relative orientations of the cameras. In the YCB-V dataset, only the real

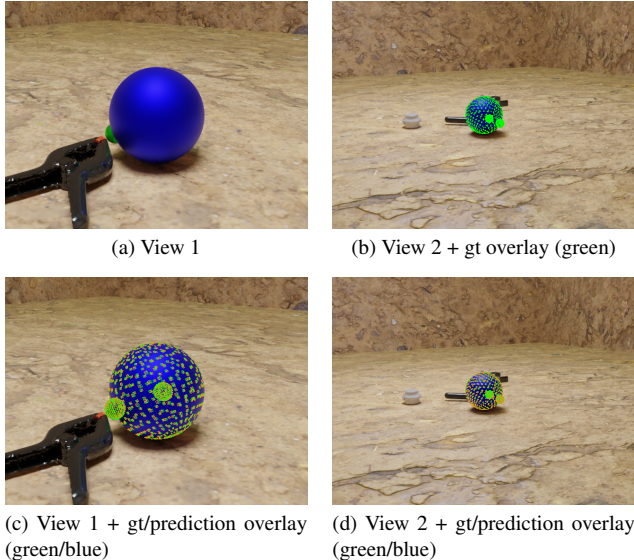


Figure 4. Example view pair of the easy test set of the MV-ball dataset. a) shows view 1 without any overlays. b) shows view 2 with the ground-truth (gt) overlay (green) only. In c) and d), both views are displayed with prediction (blue) and gt (green)

split of the training data provides the external camera parameters. We therefore only trained a single view version of our model but trained on the real and synthetic images to allow a fair comparison.

### 5.3. Implementation details

Our baseline model has 5 encoder/decoder layers, 16 heads, and an embedding dimension of 256. As the backbone, we use a Mask R-CNN [56] for the MV-ball dataset and YOLOv4 [57] for the YCB-V dataset. We used the object detector backbone only for multi-scale feature extraction and used the ground-truth labels for the bounding box information. The use of the object detector for bounding box prediction is not meaningful when evaluating the pose estimation pipeline itself. In the case of MV-ball, we added a random jitter as introduced by PoET. The lines of sight are encoded as direction + origin. We trained our baseline model for 100 epochs using the AdamW optimizer with a learning rate  $2 \times 10^{-5}$  and a batch size of 1. For YCB-V, we trained for 100 epochs at a batch size of 16. In PoET, the number of queries was set based on the maximum number of objects in an image [33]. Consequently, we used 2 queries for MV-ball and 10 for YCB-V. However, we investigated different numbers of queries in the ablations.

### 5.4. Results

The results of the MV-ball dataset can be seen in Tab. 1. We achieve a mean ADD error of 0.01185 m and a mean rotation error of  $7.345^\circ$ . Therefore, we outperform PoET and CosyPose by a large margin. Both methods do not resolve

Method	Mean ADD	Mean rot. error
PoET [33]	0.07552	95.455
CosyPose 1v [38]	1.04291	105.539
CosyPose 2v [38]	1.04312	105.539
<b>MVTOP 1v (ours)</b>	<b>0.03702</b>	<b>41.362</b>
<b>MVTOP 2v (ours)</b>	<b>0.01185</b>	<b>7.345</b>

Table 1. Results of different methods on the MV-ball dataset. The ADD error is reported in mm and the rotation error in degree. CosyPose and MVTOP are trained/evaluated with one view (1v) and two views (2v)

the pose ambiguity described in Sec. 3. For PoET, this is obvious because it is a single-view method and these methods fail by design. For CosyPose, the situation is similar since the multi-view aspect in CosyPose is based on the poses estimated from the single views. The approach of [15] cannot be evaluated on this dataset because the code is unavailable.

The qualitative results of our approach can be seen in Fig. 4. Here, the 3D model was used to generate a mesh that was projected into the 2D image using the interior orientation of the camera and the predicted/gt pose. For the sake of visibility, only every 8th mesh vertex was projected, resulting in an appearance that resembles a point cloud. In Fig. 4c and Fig. 4d, the projected prediction (blue) and the ground-truth (gt) projection (green) align so well that they barely can be distinguished. This highlights the performance of our multi-view approach. It is important to note that due to the projection of the complete 3D model into the image plane, the mesh of the hidden hemisphere is displayed although the hemisphere is not visible in the image itself. In Fig. 4a, it can be seen that only the green hemisphere (close to the black clamp) is visible. In Fig. 4c, the projection of the mesh shows that the red hemisphere (denser green/blue mesh points in the middle) is located on the other side of the ball. Conversely, in Fig. 4d, the red hemisphere would be visible (although it cannot be seen due to the overlay of gt and prediction), while the location of the green hemisphere is indicated again by the denser green/blue mesh points almost in the middle of the ball.

As described in Sec. 3, we generated two test sets of the MV-ball to investigate the influence of the visibility of the hemispheres. The results can be seen in the histogram of Fig. 5. The bin size corresponds to a step size of  $3^\circ$ . The easy set consists of 3853 images and the hard set of 3458 images. It can be seen that a higher threshold for the visibility of the hemispheres clearly reduces the rotation error, leading to a better pose estimation. For the easy test set with a threshold of 300 pixels, the highest rotation error is at  $\approx 85^\circ$  and the mean is  $\approx 3.43^\circ$  while for the hard test set with a threshold of 10 pixels the highest error is  $\approx 174^\circ$  and the mean is  $\approx 7.39^\circ$ .

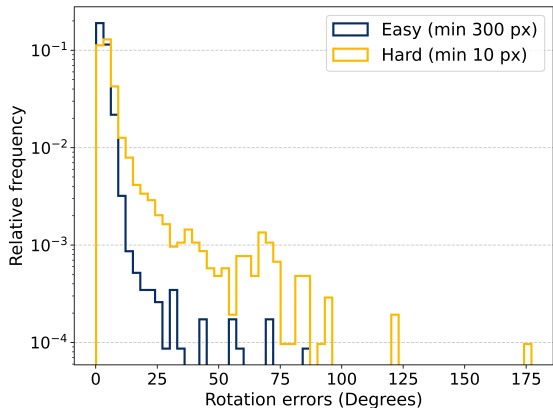


Figure 5. Histogram for the rotation errors of MVTOP on the two different test sets of the MV-ball dataset. For the easy set (blue) and the hard set (yellow), a mean rotation of  $3.43^\circ$  and  $7.39^\circ$  was reached. Note the logarithmic scale of the  $y$  axis.

The results of the YCB-V dataset can be seen in Tab. 2. We achieve SOTA results with an AUC of the ADD-S metric of 96.50. However, as discussed in section Sec. 8, the synthetic training split suffers a flaw by incorporating test information. Therefore, results of methods that are trained on the synthetic YCB-V split cannot be compared in a fair manner and might even be meaningless. In this comparison, this would apply to the methods of [15, 25, 31, 33].

Method	AUC of ADD-S
PoET [33]	92.8
T6D [31]	86.2
GDR-Net [25]	91.6
[15] 1v	75.1
[15] 5v	80.2
CosyPose 1v [38]	89.8
CosyPose 5v [38]	93.4
<b>MVTOP 1v (ours)</b>	<b>96.50</b>

Table 2. Results of different methods on the YCB-V dataset using the AUC of ADD-S metric.

### 5.5. Runtime analysis

The runtime analysis was performed on the YCB-V dataset with a model only trained on the real-data training split since we could test different numbers of views. We measured the inference time per image. To reduce the influence of processes like initialization, data loading, etc. on the mean value, we averaged five runs per test. As the test set, we used the subset of the YCB-V testset proposed by the BOP-Challenge [13], which consists of 75 images from

# Views	GPU 1	GPU 2	CosyPose	T6D
1	82.90	69.97		170
2	131.51	100.96		
4	224.66	163.39	320	

Table 3. Runtime analysis (in ms) for a Nvidia GTX 1080 (GPU 1) and a Nvidia RTX 3080 (GPU 2). The analysis was conducted for 1,2,4 and 8 views.

each of the 12 test scenes totaling 900 validation images at a resolution of  $640 \times 480$  pixels with a total of 4125 annotations. Therefore, each image contained on average  $\approx 4.6$  objects. For comparison, we cite the runtime of CosyPose and T6D as described in the papers [31, 38]. It is important to note that a complete and fair comparison cannot be made because it is not stated in [31, 38] which hardware was used and on which dataset or which image size the analysis was performed. However, our tests indicate that our model runs at a competitive speed.

## 6. Ablations

The ablations were performed on the MV-ball dataset. While in PoET [33] a classical encoder-decoder approach was used, [52] only used a decoder that operates directly on the feature maps. Therefore, we investigated the influence of the encoder and present the results in Tab. 4. It can be seen that without the encoder, the mean ADD and rotation error increase. This shows the strong contribution of the encoder in generating meaningful embeddings of view-specific features.

encoder	mean ADD	mean Rotation Error
w/	0.01185	7.345
w/o	0.03287	33.667

Table 4. Effect of the encoder in the MVTOP network

As described in Sec. 4, the model is enriched with the embedding of the lines of sight (LoS) of the different views. However, there are several ways to encode the LoS. Our baseline encoded them as the origin and direction of the vectors for the pixels. Our ablations include three additional encoding approaches. That is, just giving the direction of the rays, encoding the rays via the Plücker coordinates, and passing the Plücker coordinates and the origin. The Plücker coordinates consist of the direction of the rays and the so-called moment, which is calculated as the vector product of the direction of the ray and one point lying on the ray and by using the origin as this point the moment can be calculated as follows [58]:

$$\mathbf{m} = \vec{\mathbf{a}} \times \vec{\mathbf{b}} \quad (8)$$



(a) Image 000048/000002 of the YCB-V test split



(b) Image 000002/002468 of the YCB-V synthetic split

Figure 6. Qualitative comparison of the test split and the synthetic split of the YCB-V dataset. The poses of the red cup are practically identical.

LoS encoding	Mean ADD	Mean rot. error
baseline	0.01185	7.345
dir only	0.01387	10.267
Pl. coord.	0.014	10.858
Pl. coord. + orig	<b>0.01042</b>	<b>6.211</b>

Table 5. Influence of different LoS encodings. From top to bottom: direction + origin, direction only, Plücker coordinates and Plücker coordinates + origin

Tab. 5 shows the results of the different LoS encodings. It can be seen that the mean ADD and rotation error do not vary much with respect to the baseline. While passing the origin alone or Plücker coordinates worsened the errors, the performance of our model could be increased somewhat by passing Plücker coordinates plus the origin. We assume that, although the origin is encoded in the moment of the Plücker coordinates, the model benefits from the direct access to the origin and does not have to learn to unravel the vector product.

A key component of the transformer are the queries for which the model makes its prediction. Consequently, the number of queries defines the upper bound of the number of objects to detect. In the original Deformable-DETR setup [34], the number of queries was set to 300, which led to an accuracy on the COCO dataset of 43.2%. In [59], the queries were increased, to 900 which led to an accuracy of 45.4%. This indicates that more queries can lead to better performance. In PoET, the number of queries was set as the maximum number of objects that can appear in an image plus one additional query. Because the YCB-V dataset has

at most nine objects in an image, the number of queries in PoET was set to ten. We wanted to investigate whether the number of queries plays a crucial role with respect to accuracy. Corresponding to PoET, we started from our baseline, which used two queries since the MV-ball dataset always contained one ball per image. We examined four other implementations, namely with one query, four queries, and eight queries. The results can be seen in Tab. 6.

# queries	Mean ADD	Mean rot. error
baseline (2)	0.01185	7.345
1	0.01089	<b>6.904</b>
4	0.01091	7.139
8	<b>0.0095664</b>	7.139

Table 6. Influence of the number of queries

It can be seen that the errors barely change. Furthermore, the best results differ depending on the metric used. While the relative difference in the number of queries corresponds to the mentioned works above (a factor of 2–4), the absolute change is small.

## 7. Limitations

As described in Sec. 4, our method defines queries based on the bounding boxes of a reference image. The prediction is made for these queries, i.e., only for the first image. All other images/views provide only additional information, which means that no prediction is made for these images directly. As mentioned in Sec. 4, we only work with the gt annotations; therefore, no detections are missed. With a detector, this would not reflect reality due to, e.g., occlusions.

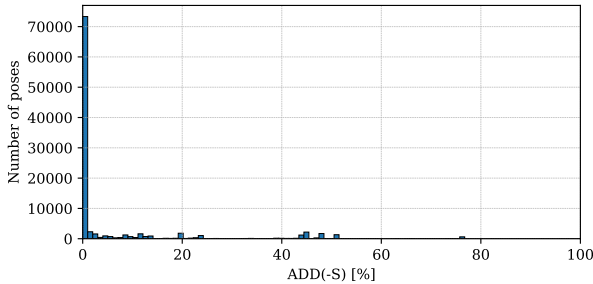


Figure 7. Comparison of all test poses with all poses of the synthetic training split taking the object ID into account. The histogram shows the distribution of test poses with respect to the difference in the ADD-(S) metric to the nearest matching pose. The x-axis has a bin size of 1%.

This could lead to the situation where the reference image only has three detections while an additional image/view has six detections. This could be fixed by generating the queries/input based on the number of detections of the images.

Furthermore, it would be possible that a camera setup generates several non-overlapping areas. Therefore, it would be possible to have, e.g., two objects in two different non-overlapping regions. Both views could only detect one object and a generation of the queries based on the number of detections would not lead to more possible true predictions. In this case, the queries would need to be generated for every view, so predictions are made for every view separately. On one hand, this would ensure that objects that fall into such non-overlapping regions can also be found, while on the other hand, the computational cost would scale with the number of views. This can be useful depending on the setup and task. In short, in this case, our method would always miss detections of certain areas, depending on the reference view.

## 8. YCB-V Training Data Flaw

During our experiments we found a potentially critical flaw in the YCB-V training dataset (“train\_synth”). A significant amount of the object poses in the synthetic training images were taken from the test set. The objects are not cut out from the test set, but are rendered from the 3D-model, which results in a similar appearance as can be seen in Fig. 6. The translation and rotation of the cup in the image from test split differ from the cup in the image from the synthetic split in Fig. 6 by  $5.29623 \times 10^{-4}$  mm and  $7.426 \times 10^{-5}$  degrees. This indeed indicates that the exact poses from the test set were taken to generate poses for the synthetic set.

To highlight our observations, we numerically investigated the individual poses. We compared all translation

vectors of an object ID in the test set with all vectors of the same object ID in the synthetic dataset. With a maximum distance of both vectors of 0.01 mm, we found that  $\approx 30\%$  of the poses in the test set have a duplicate in the synthetic set which corresponds to  $\approx 8\%$  of the poses of the synthetic set being taken as poses from the test split. The same applies for the real training split of the YCB-V dataset. We found that  $\approx 32\%$  of the poses in the training set have a duplicate in the synthetic dataset, which corresponds to  $\approx 59\%$  of the poses of the synthetic set being taken as poses from the real split. In total,  $\approx 67\%$  of the synthetic poses are either taken from the test set or the real set with respect to the translation error and the mentioned threshold. We used this threshold since it corresponds to float precision with respect to the typical size of the translations which lie in the range of 1000 mm. We also examined the ADD difference of the poses found with the aforementioned translation threshold. In Fig. 7, the histogram of the differences in the ADD metric of the poses is displayed with a bin size of 1%. Over 70,000 poses from the test set have a duplicate pose in the synthetic training set with an ADD difference of at most 1%. With 98,567 poses in total, this corresponds to over 71%. Therefore, the synthetic training set is heavily corrupted by information from the test set. A method that overfits and only produces poses from the training set could still find over 70% of all test poses correctly.

To the best of our knowledge, this has not been acknowledged since the dataset was introduced eight years ago. This means that methods that were also trained on this synthetic data split are not trained correctly and cannot be compared in a fair manner with each other and especially not with methods that do not use this data at all. This renders the corresponding results on this dataset meaningless.

## 9. Conclusion

In this work, we presented a novel multi-view pose estimation network. The attention-based encoder-decoder approach fuses multi-view features and enriches the embeddings with line-of-sight information. This enables the model to establish a strong understanding of the scene.

Furthermore, we created the MV-ball dataset that allows us to benchmark pose estimation methods with respect to their multi-view capability. The poses of the instances in the dataset can only be determined if the view-specific information is combined before the actual pose estimation.

Our method MVTOP can resolve the mentioned pose ambiguity and outperforms existing pose estimation methods on this task. As far as we know, no other existing method can resolve such pose ambiguities consistently. Furthermore, our approach achieves SOTA results on the well-established YCB-V dataset. However, the evaluation results on the YCB-V dataset might only be of limited use because of the flaw in the dataset we pointed out in this work as well.

## References

- [1] Benjamin Busam, Marco Esposito, Simon Che'Rose, Nassir Navab, and Benjamin Frisch. A Stereo Vision Approach for Cooperative Robotic Movement Therapy. In *2015 IEEE International Conference on Computer Vision Workshop (ICCVW)*, pages 519–527, December 2015. doi: 10.1109/ICCVW.2015.74. URL <https://ieeexplore.ieee.org/document/7406423>. 1
- [2] Bowen Wen, Wenzhao Lian, Kostas Bekris, and Stefan Schaal. CaTGrasp: Learning Category-Level Task-Relevant Grasping in Clutter from Simulation. In *2022 International Conference on Robotics and Automation (ICRA)*, pages 6401–6408, Philadelphia, PA, USA, May 2022. IEEE Press. doi: 10.1109/ICRA46639.2022.9811568. URL <https://doi.org/10.1109/ICRA46639.2022.9811568>.
- [3] Ghazal Ghazaei, Iro Laina, Christian Rupprecht, Federico Tombari, Nassir Navab, and Kianoush Nazarpour. Dealing with Ambiguity in Robotic Grasping via Multiple Predictions. In *Computer Vision – ACCV 2018: 14th Asian Conference on Computer Vision, Perth, Australia, December 2–6, 2018, Revised Selected Papers, Part IV*, pages 38–55, Berlin, Heidelberg, December 2018. Springer-Verlag. ISBN 978-3-030-20869-1. doi: 10.1007/978-3-030-20870-7\_3. URL [https://doi.org/10.1007/978-3-030-20870-7\\_3](https://doi.org/10.1007/978-3-030-20870-7_3).
- [4] Jonathan Tremblay, Thang To, Balakumar Sundaralingam, Yu Xiang, Dieter Fox, and Stan Birchfield. Deep Object Pose Estimation for Semantic Robotic Grasping of Household Objects. In *Proceedings of The 2nd Conference on Robot Learning*, pages 306–316. PMLR, October 2018. URL <https://proceedings.mlr.press/v87/tremblay18a.html>. ISSN: 2640-3498.
- [5] Daniel Kappler, Franziska Meier, Jan Issac, Jim Mainprice, Cristina Garcia Cifuentes, Manuel Wüthrich, Vincent Berenz, Stefan Schaal, Nathan Ratliff, and Jeannette Bohg. Real-Time Perception Meets Reactive Motion Generation. *IEEE Robotics and Automation Letters*, 3(3):1864–1871, July 2018. ISSN 2377-3766. doi: 10.1109/LRA.2018.2795645. URL <https://ieeexplore.ieee.org/document/8263622>.
- [6] Menglong Zhu, Konstantinos G. Derpanis, Yinfei Yang, Samarth Brahmhatt, Mabel Zhang, Cody Phillips, Matthieu Lecce, and Kostas Daniilidis. Single image 3D object detection and pose estimation for grasping. In *2014 IEEE International Conference on Robotics and Automation (ICRA)*, pages 3936–3943, May 2014. doi: 10.1109/ICRA.2014.6907430. URL <https://ieeexplore.ieee.org/document/6907430>. ISSN: 1050-4729.
- [7] Alvaro Collet, Manuel Martinez, and Siddhartha S Srinivasa. The MOPED framework: Object recognition and pose estimation for manipulation. *The International Journal of Robotics Research*, 30(10):1284–1306, September 2011. ISSN 0278-3649, 1741-3176. doi: 10.1177/0278364911401765. URL <https://journals.sagepub.com/doi/10.1177/0278364911401765>. 1
- [8] Fulin Tang, Yihong Wu, Xiaohui Hou, and Haibin Ling. 3D Mapping and 6D Pose Computation for Real Time Augmented Reality on Cylindrical Objects. *IEEE Transactions on Circuits and Systems for Video Technology*, 30(9):2887–2899, September 2020. ISSN 1558-2205. doi: 10.1109/TCSVT.2019.2950449. URL <https://ieeexplore.ieee.org/document/8887213>. 1
- [9] Jason Rambach, Alain Pagani, Michael Schneider, Oleksandr Artemenko, and Didier Stricker. 6DoF Object Tracking based on 3D Scans for Augmented Reality Remote Live Support. *Computers*, 7(1):6, March 2018. ISSN 2073-431X. doi: 10.3390/computers7010006. URL <https://www.mdpi.com/2073-431X/7/1/6>. Number: 1 Publisher: Multidisciplinary Digital Publishing Institute.
- [10] Eric Marchand, Hideaki Uchiyama, and Fabien Spindler. Pose Estimation for Augmented Reality: A Hands-On Survey. *IEEE Transactions on Visualization and Computer Graphics*, 22(12):2633–2651, December 2016. ISSN 1941-0506. doi: 10.1109/TVCG.2015.2513408. URL <https://ieeexplore.ieee.org/document/7368948>. 1
- [11] Di Wu, Zhaoyong Zhuang, Canqun Xiang, Wenbin Zou, and Xia Li. 6D-VNet: End-To-End 6DoF Vehicle Pose Estimation From Monocular RGB Images. In *2019 IEEE/CVF Conference on Computer Vision and Pattern Recognition Workshops (CVPRW)*, pages 1238–1247, Long Beach, CA, USA, June 2019. IEEE. ISBN 978-1-7281-2506-0. doi: 10.1109/CVPRW.2019.00163. URL <https://ieeexplore.ieee.org/document/9025591>. 1
- [12] Luis Pérez, Íñigo Rodríguez, Nuria Rodríguez, Rubén Usamentiaga, and Daniel F. García. Robot Guidance Using Machine Vision Techniques in Industrial Environments: A Comparative Review. *Sensors*, 16(3):335, March 2016. ISSN 1424-8220. doi: 10.3390/s16030335. URL <https://www.mdpi.com/1424-8220/16/3/335>. Number: 3 Publisher: Multidisciplinary Digital Publishing Institute. 1
- [13] Tomáš Hodaň, Martin Sundermeyer, Bertram Drost, Yann Labbé, Eric Brachmann, Frank Michel, Carsten Rother, and Jiří Matas. BOP Challenge 2020 on 6D Object Localization. In *Computer Vision – ECCV 2020 Workshops: Glasgow, UK, August 23–28, 2020, Proceedings, Part II*, pages 577–594, Berlin, Heidelberg, August 2020. Springer-Verlag. ISBN 978-3-030-66095-6. doi: 10.1007/978-3-030-66096-3\_39. URL [https://doi.org/10.1007/978-3-030-66096-3\\_39](https://doi.org/10.1007/978-3-030-66096-3_39). 1, 3, 5, 7
- [14] Van Nguyen Nguyen, Stephen Tyree, Andrew Guo, Mederic Fourmy, Anas Gouda, Taeyeop Lee, Sungphill Moon, Hyeontae Son, Lukas Ranftl, Jonathan Tremblay, Eric Brachmann, Bertram Drost, Vincent Lepetit, Carsten Rother, Stan Birchfield, Jiri Matas, Yann Labbe, Martin Sundermeyer, and Tomas Hodan. BOP Challenge 2024 on Model-Based and Model-Free 6D Object Pose Estimation, April 2025. URL <http://arxiv.org/abs/2504.02812>. arXiv:2504.02812 [cs]. 1, 3, 5
- [15] Chi Li, Jin Bai, and Gregory D. Hager. A Unified Framework for Multi-view Multi-class Object Pose Estimation. In *Computer Vision – ECCV 2018: 15th European Conference, Munich, Germany, September 8-14, 2018, Proceedings, Part XVI*, pages 263–281, Berlin, Heidelberg, September 2018. Springer-Verlag. ISBN 978-3-030-01269-4. doi:

- 10.1007/978-3-030-01270-0\_16. URL [https://doi.org/10.1007/978-3-030-01270-0\\_16](https://doi.org/10.1007/978-3-030-01270-0_16). 2, 3, 6, 7
- [16] Ashish Vaswani, Noam Shazeer, Niki Parmar, Jakob Uszkoreit, Llion Jones, Aidan N. Gomez, Łukasz Kaiser, and Illia Polosukhin. Attention is all you need. In *Proceedings of the 31st International Conference on Neural Information Processing Systems, NIPS'17*, pages 6000–6010, Red Hook, NY, USA, December 2017. Curran Associates Inc. ISBN 978-1-5108-6096-4. 2
- [17] Wadim Kehl, Fabian Manhardt, Federico Tombari, Slobodan Ilic, and Nassir Navab. SSD-6D: Making RGB-Based 3D Detection and 6D Pose Estimation Great Again. In *2017 IEEE International Conference on Computer Vision (ICCV)*, pages 1530–1538, October 2017. doi: 10.1109/ICCV.2017.169. URL <https://ieeexplore.ieee.org/document/8237431/footnotes>. ISSN: 2380-7504. 2
- [18] Gu Wang, Fabian Manhardt, Jianzhun Shao, Xiangyang Ji, Nassir Navab, and Federico Tombari. Self6D: 16th European Conference on Computer Vision, ECCV 2020. *Computer Vision – ECCV 2020 - 16th European Conference, 2020, Proceedings*, pages 108–125, 2020. ISSN 9783030584511. doi: 10.1007/978-3-030-58452-8\_7. URL <http://www.scopus.com/inward/record.url?scp=85097242845&partnerID=8YFLogxK>. Publisher: Springer Science and Business Media Deutschland GmbH.
- [19] Yu Xiang, Tanner Schmidt, Venkatraman Narayanan, and Dieter Fox. PoseCNN: A Convolutional Neural Network for 6D Object Pose Estimation in Cluttered Scenes. In *Proceedings of Robotics: Science and Systems*, volume 14, Pittsburgh, Pennsylvania, June 2018. ISBN 978-0-9923747-4-7. doi: 10.15607/RSS.2018.XIV.019. URL <https://www.roboticsproceedings.org/rss14/p19.html>. 2, 3, 5
- [20] Juil Sock, Guillermo Garcia-Hernando, Anil Armagan, and Tae-Kyun Kim. Introducing Pose Consistency and Warp-Alignment for Self-Supervised 6D Object Pose Estimation in Color Images. In *2020 International Conference on 3D Vision (3DV)*, pages 291–300, November 2020. doi: 10.1109/3DV50981.2020.00039. URL <https://ieeexplore.ieee.org/document/9320376>. ISSN: 2475-7888. 2
- [21] Kartik Gupta, Lars Petersson, and Richard Hartley. CullNet: Calibrated and pose aware confidence scores for object pose estimation. In *2019 IEEE/CVF international conference on computer vision workshop (ICCVW)*, pages 2758–2766, Los Alamitos, CA, USA, October 2019. IEEE Computer Society. doi: 10.1109/ICCVW.2019.00337. URL <https://doi.ieeecomputersociety.org/10.1109/ICCVW.2019.00337>. 2
- [22] Sergey Zakharov, Ivan Shugurov, and Slobodan Ilic. DPOD: 6D Pose Object Detector and Refiner. In *2019 IEEE/CVF International Conference on Computer Vision (ICCV)*, pages 1941–1950, October 2019. doi: 10.1109/ICCV.2019.00203. URL <https://ieeexplore.ieee.org/document/9010850>. ISSN: 2380-7504.
- [23] Kiru Park, Timothy Patten, and Markus Vincze. Pix2Pose: Pixel-Wise Coordinate Regression of Objects for 6D Pose Estimation. In *2019 IEEE/CVF International Conference on Computer Vision (ICCV)*, pages 7667–7676, October 2019. doi: 10.1109/ICCV.2019.00776. URL <https://ieeexplore.ieee.org/document/9008819>. ISSN: 2380-7504.
- [24] Tomáš Hodaň, Dániel Baráth, and Jiří Matas. EPOS: Estimating 6D Pose of Objects With Symmetries. In *2020 IEEE/CVF Conference on Computer Vision and Pattern Recognition (CVPR)*, pages 11700–11709, June 2020. doi: 10.1109/CVPR42600.2020.01172. URL <https://ieeexplore.ieee.org/document/9157391>. ISSN: 2575-7075.
- [25] Gu Wang, Fabian Manhardt, Federico Tombari, and Xiangyang Ji. GDR-Net: Geometry-Guided Direct Regression Network for Monocular 6D Object Pose Estimation. In *2021 IEEE/CVF Conference on Computer Vision and Pattern Recognition (CVPR)*, pages 16606–16616, June 2021. doi: 10.1109/CVPR46437.2021.01634. URL <https://ieeexplore.ieee.org/document/9578682>. ISSN: 2575-7075. 7
- [26] Yan Di, Fabian Manhardt, Gu Wang, Xiangyang Ji, Nassir Navab, and Federico Tombari. SO-Pose: Exploiting Self-Occlusion for Direct 6D Pose Estimation. In *2021 IEEE/CVF International Conference on Computer Vision (ICCV)*, pages 12376–12385, October 2021. doi: 10.1109/ICCV48922.2021.01217. URL <https://ieeexplore.ieee.org/document/9711086>. ISSN: 2380-7504. 2
- [27] Martin Sundermeyer, Zoltan-Csaba Marton, Maximilian Durner, Manuel Brucker, and Rudolph Triebel. Implicit 3D Orientation Learning for 6D Object Detection from RGB Images. In *Computer Vision – ECCV 2018: 15th European Conference, Munich, Germany, September 8–14, 2018, Proceedings, Part VI*, pages 712–729, Berlin, Heidelberg, September 2018. Springer-Verlag. ISBN 978-3-030-01230-4. doi: 10.1007/978-3-030-01231-1\_43. URL [https://doi.org/10.1007/978-3-030-01231-1\\_43](https://doi.org/10.1007/978-3-030-01231-1_43). 2
- [28] Van Nguyen Nguyen, Yinlin Hu, Yang Xiao, Mathieu Salzmann, and Vincent Lepetit. Templates for 3D Object Pose Estimation Revisited: Generalization to New Objects and Robustness to Occlusions. In *2022 IEEE/CVF Conference on Computer Vision and Pattern Recognition (CVPR)*, pages 6761–6770, New Orleans, LA, USA, June 2022. IEEE. ISBN 978-1-6654-6946-3. doi: 10.1109/CVPR52688.2022.00665. URL <https://ieeexplore.ieee.org/document/9879950/>. 2
- [29] Stefan Hinterstoisser, Cedric Cagniart, Slobodan Ilic, Peter Sturm, Nassir Navab, Pascal Fua, and Vincent Lepetit. Gradient Response Maps for Real-Time Detection of Textureless Objects. *IEEE Transactions on Pattern Analysis and Machine Intelligence*, 34(5):876–888, May 2012. ISSN 1939-3539. doi: 10.1109/TPAMI.2011.206. URL <https://ieeexplore.ieee.org/document/6042881>. 2
- [30] Yongzhi Su, Mahdi Saleh, Torben Fetzter, Jason Rambach, Nassir Navab, Benjamin Busam, Didier Stricker, and Federico Tombari. ZebraPose: 2022 IEEE/CVF Conference on Computer Vision and Pattern Recognition, CVPR 2022. *Proceedings - 2022 IEEE/CVF Conference on Computer Vision and Pattern Recognition, CVPR 2022*, pages 6728–

- 6738, 2022. doi: 10.1109/CVPR52688.2022.00662. URL <http://www.scopus.com/inward/record.url?scp=85136707551&partnerID=8YFLogxK>. Publisher: IEEE Computer Society. 2
- [31] Arash Amini, Arul Selvam Periyasamy, and Sven Behnke. T6D-direct: Transformers for multi-object 6D pose direct regression. In Christian Bauckhage, Juergen Gall, and Alexander Schwing, editors, *Pattern recognition*, pages 530–544, Cham, 2021. Springer International Publishing. ISBN 978-3-030-92659-5. 2, 7
- [32] Nicolas Carion, Francisco Massa, Gabriel Synnaeve, Nicolas Usunier, Alexander Kirillov, and Sergey Zagoruyko. End-to-End Object Detection with Transformers. In *Computer Vision – ECCV 2020: 16th European Conference, Glasgow, UK, August 23–28, 2020, Proceedings, Part I*, pages 213–229, Berlin, Heidelberg, August 2020. Springer-Verlag. ISBN 978-3-030-58451-1. doi: 10.1007/978-3-030-58452-8\_13. URL [https://doi.org/10.1007/978-3-030-58452-8\\_13](https://doi.org/10.1007/978-3-030-58452-8_13). 2, 3
- [33] Thomas Georg Jantos, Mohamed Amin Hamdad, Wolfgang Granig, Stephan Weiss, and Jan Steinbrener. PoET: Pose Estimation Transformer for Single-View, Multi-Object 6D Pose Estimation. In *Proceedings of The 6th Conference on Robot Learning*, pages 1060–1070. PMLR, March 2023. URL <https://proceedings.mlr.press/v205/jantos23a.html>. ISSN: 2640-3498. 2, 3, 4, 5, 6, 7
- [34] Xizhou Zhu, Weijie Su, Lewei Lu, Bin Li, Xiaogang Wang, and Jifeng Dai. Deformable DETR: deformable transformers for end-to-end object detection. In *9th international conference on learning representations, ICLR 2021, virtual event, austria, may 3-7, 2021*. OpenReview.net, 2021. URL <https://openreview.net/forum?id=gZ9hCDWe6ke>. tex.bibsource: dblp computer science bibliography, <https://dblp.org> tex.timestamp: Tue, 15 Nov 2022 12:11:35 +0100. 2, 3, 5, 8
- [35] Andy Zeng, Kuan-Ting Yu, Shuran Song, Daniel Suo, Ed Walker, Alberto Rodriguez, and Jianxiong Xiao. Multi-view self-supervised deep learning for 6D pose estimation in the Amazon Picking Challenge. In *2017 IEEE International Conference on Robotics and Automation (ICRA)*, pages 1386–1383, Singapore, Singapore, May 2017. IEEE Press. doi: 10.1109/ICRA.2017.7989165. URL <https://doi.org/10.1109/ICRA.2017.7989165>. 2
- [36] Fabian Duffhauss, Tobias Demmler, and Gerhard Neumann. MV6D: Multi-View 6D Pose Estimation on RGB-D Frames Using a Deep Point-wise Voting Network. In *2022 IEEE/RSJ International Conference on Intelligent Robots and Systems (IROS)*, pages 3568–3575, October 2022. doi: 10.1109/IROS47612.2022.9982268. URL <https://ieeexplore.ieee.org/document/9982268>. ISSN: 2153-0866.
- [37] Juil Sock, S. Hamidreza Kasaei, Luis Seabra Lopes, and Tae-Kyun Kim. Multi-view 6D Object Pose Estimation and Camera Motion Planning Using RGBD Images. In *2017 IEEE International Conference on Computer Vision Workshops (ICCVW)*, pages 2228–2235, October 2017. doi: 10.1109/ICCVW.2017.260. URL <https://ieeexplore.ieee.org/document/8265470>. ISSN: 2473-9944. 2
- [38] Yann Labbé, Justin Carpentier, Mathieu Aubry, and Josef Sivic. CosyPose: Consistent Multi-view Multi-object 6D Pose Estimation. In *Computer Vision – ECCV 2020: 16th European Conference, Glasgow, UK, August 23–28, 2020, Proceedings, Part XVII*, pages 574–591, Berlin, Heidelberg, August 2020. Springer-Verlag. ISBN 978-3-030-58519-8. doi: 10.1007/978-3-030-58520-4\_34. URL [https://doi.org/10.1007/978-3-030-58520-4\\_34](https://doi.org/10.1007/978-3-030-58520-4_34). 2, 5, 6, 7
- [39] Eric Brachmann, Alexander Krull, Frank Michel, Stefan Gumhold, Jamie Shotton, and Carsten Rother. Learning 6D Object Pose Estimation Using 3D Object Coordinates. In David Fleet, Tomas Pajdla, Bernt Schiele, and Tinne Tuytelaars, editors, *Computer Vision – ECCV 2014*, pages 536–551, Cham, 2014. Springer International Publishing. ISBN 978-3-319-10605-2. doi: 10.1007/978-3-319-10605-2\_35. 3
- [40] Tomas Hodan, Pavel Haluza, Stepan Obdrzalek, Jiri Matas, Manolis Lourakis, and Xenophon Zabulis. T-LESS: An RGB-d dataset for 6D pose estimation of texture-less objects. In *2017 IEEE winter conference on applications of computer vision (WACV)*, pages 880–888, Los Alamitos, CA, USA, March 2017. IEEE Computer Society. doi: 10.1109/WACV.2017.103. URL <https://doi.ieeecomputersociety.org/10.1109/WACV.2017.103>. 3
- [41] Bertram Drost, Markus Ulrich, Paul Bergmann, Philipp Härtinger, and Carsten Steger. Introducing MVTEC ITODD — A Dataset for 3D Object Recognition in Industry. In *2017 IEEE International Conference on Computer Vision Workshops (ICCVW)*, pages 2200–2208, October 2017. doi: 10.1109/ICCVW.2017.257. URL <https://ieeexplore.ieee.org/document/8265467>. ISSN: 2473-9944. 3
- [42] Roman Kaskman, Sergey Zakharov, Ivan Shugurov, and Slobodan Ilic. HomebrewedDB: RGB-D Dataset for 6D Pose Estimation of 3D Objects. In *2019 IEEE/CVF International Conference on Computer Vision Workshop (ICCVW)*, pages 2767–2776, October 2019. doi: 10.1109/ICCVW.2019.00338. URL <https://ieeexplore.ieee.org/document/9021987>. ISSN: 2473-9944. 3
- [43] Andreas Doumanoglou, Rigas Kouskouridas, Sotiris Malasiotis, and Tae-Kyun Kim. Recovering 6D Object Pose and Predicting Next-Best-View in the Crowd. In *2016 IEEE Conference on Computer Vision and Pattern Recognition (CVPR)*, pages 3583–3592, June 2016. doi: 10.1109/CVPR.2016.390. URL <https://ieeexplore.ieee.org/document/7780759>. ISSN: 1063-6919. 3
- [44] Tomáš Hodaň, Frank Michel, Eric Brachmann, Wadim Kehl, Anders Glent Buch, Dirk Kraft, Bertram Drost, Joel Vidal, Stephan Ihrke, Xenophon Zabulis, Caner Sahin, Fabian Manhardt, Federico Tombari, Tae-Kyun Kim, Jiří Matas, and Carsten Rother. BOP: Benchmark for 6D object pose estimation. In Vittorio Ferrari, Martial Hebert, Cristian Sminchisescu, and Yair Weiss, editors, *Computer vision – ECCV 2018*, pages 19–35, Cham, 2018. Springer International Publishing. ISBN 978-3-030-01249-6. 3
- [45] Stephen Tyree, Jonathan Tremblay, Thang To, Jia Cheng, Terry Mosier, Jeffrey Smith, and Stan Birchfield. 6-DoF

- Pose Estimation of Household Objects for Robotic Manipulation: An Accessible Dataset and Benchmark. In *2022 IEEE/RSJ International Conference on Intelligent Robots and Systems (IROS)*, pages 13081–13088, October 2022. doi: 10.1109/IROS47612.2022.9981838. URL <https://ieeexplore.ieee.org/document/9981838>. ISSN: 2153-0866. 3
- [46] Andrew Guo, Bowen Wen, Jianhe Yuan, Jonathan Tremblay, Stephen Tyree, Jeffrey Smith, and Stan Birchfield. HANDAL: A Dataset of Real-World Manipulable Object Categories with Pose Annotations, Affordances, and Reconstructions. In *IROS*, pages 11428–11435, 2023. doi: 10.1109/IROS55552.2023.10341672. 3
- [47] Prithviraj Banerjee, Sindi Shkodrani, Pierre Moulon, Shreyas Hampali, Shangchen Han, Fan Zhang, Linguang Zhang, Jade Fountain, Edward Miller, Selen Basol, Richard Newcombe, Robert Wang, Jakob Julian Engel, and Tomas Hodan. HOT3D: Hand and object tracking in 3D from ego-centric multi-view videos. In *Proceedings of the computer vision and pattern recognition conference (CVPR)*, pages 7061–7071, June 2025. 3
- [48] Junwen Huang, Jizhong Liang, Jiaqi Hu, Martin Sundermeyer, Peter KT Yu, Nassir Navab, and Benjamin Busam. XYZ-IBD: High-precision Bin-picking Dataset for Object 6D Pose Estimation Capturing Real-world Industrial Complexity, May 2025. URL <https://arxiv.org/abs/2506.00599v1>. 3
- [49] Agastya Kalra, Guy Stoppi, Dmitrii Marin, Vage Taamazyan, Aarrushi Shandilya, Rishav Agarwal, Anton Boykov, Tze Hao Chong, and Michael Stark. Towards co-evaluation of cameras, HDR, and algorithms for industrial-grade 6DoF pose estimation. In *2024 IEEE/CVF conference on computer vision and pattern recognition (CVPR)*, pages 22691–22701, 2024. doi: 10.1109/CVPR52733.2024.02141. 3
- [50] Jun Yang, Yizhou Gao, Dong Li, and Steven L. Waslander. ROBI: A Multi-View Dataset for Reflective Objects in Robotic Bin-Picking. In *2021 IEEE/RSJ International Conference on Intelligent Robots and Systems (IROS)*, pages 9788–9795, September 2021. doi: 10.1109/IROS51168.2021.9635871. URL <https://ieeexplore.ieee.org/document/9635871>. ISSN: 2153-0866. 3
- [51] Maximilian Denninger, Martin Sundermeyer, Dominik Winkelbauer, Dmitry Olefir, Tomas Hodan, Youssef Zidan, Mohamad Elbadrawy, Markus Knauer, Harinandan Katam, and Ahsan Lodhi. BlenderProc: Reducing the Reality Gap with Photorealistic Rendering. In *16th Robotics: Science and Systems, RSS 2020, Workshops, Virtuall*, July 2020. ISBN 978-0-9923747-6-1. URL <https://elib.dlr.de/139317/>. ISSN: 2330765X. 3
- [52] Tao Wang, Jianfeng Zhang, Yujun Cai, Shuicheng Yan, and Jiashi Feng. Direct multi-view multi-person 3D pose estimation. In *Proceedings of the 35th International Conference on Neural Information Processing Systems, NIPS '21*, pages 13153–13164, Red Hook, NY, USA, December 2021. Curran Associates Inc. ISBN 978-1-7138-4539-3. 3, 4, 5, 7
- [53] Yi Zhou, Connelly Barnes, Jingwan Lu, Jimei Yang, and Hao Li. On the Continuity of Rotation Representations in Neural Networks. In *2019 IEEE/CVF Conference on Computer Vision and Pattern Recognition (CVPR)*, pages 5738–5746, June 2019. doi: 10.1109/CVPR.2019.00589. URL <https://ieeexplore.ieee.org/document/8953486>. ISSN: 2575-7075. 5
- [54] Stefan Hinterstoisser, Vincent Lepetit, Slobodan Ilic, Stefan Holzer, Gary Bradski, Kurt Konolige, and Nassir Navab. Model based training, detection and pose estimation of texture-less 3d objects in heavily cluttered scenes. In *Proceedings of the 11th Asian conference on Computer Vision - Volume Part I*, volume Part I of *ACCV'12*, pages 548–562, Berlin, Heidelberg, November 2012. Springer-Verlag. ISBN 978-3-642-37330-5. doi: 10.1007/978-3-642-37331-2\_42. URL [https://doi.org/10.1007/978-3-642-37331-2\\_42](https://doi.org/10.1007/978-3-642-37331-2_42). 5
- [55] Gideon Billings and Matthew Johnson-Roberson. SilhoNet: An RGB Method for 6D Object Pose Estimation. *IEEE Robotics and Automation Letters*, 4(4):3727–3734, October 2019. ISSN 2377-3766, 2377-3774. doi: 10.1109/LRA.2019.2928776. URL <http://arxiv.org/abs/1809.06893>. arXiv:1809.06893 [cs]. 5
- [56] Kaiming He, Georgia Gkioxari, Piotr Dollár, and Ross Girshick. Mask R-CNN. In *2017 IEEE International Conference on Computer Vision (ICCV)*, pages 2980–2988, October 2017. doi: 10.1109/ICCV.2017.322. URL <https://ieeexplore.ieee.org/document/8237584>. ISSN: 2380-7504. 6
- [57] Chien-Yao Wang, Alexey Bochkovskiy, and Hong-Yuan Mark Liao. Scaled-YOLOv4: Scaling Cross Stage Partial Network. In *2021 IEEE/CVF Conference on Computer Vision and Pattern Recognition (CVPR)*, pages 13024–13033, June 2021. doi: 10.1109/CVPR46437.2021.01283. URL <https://ieeexplore.ieee.org/document/9577489>. ISSN: 2575-7075. 6
- [58] Leo Dorst, Daniel Fontijne, and Stephen Mann. *Geometric algebra for computer science: an object-oriented approach to geometry*. Morgan Kaufmann series in computer graphics. Elsevier Morgan Kaufmann, Amsterdam San Francisco, 2007. ISBN 978-0-12-369465-2 978-0-12-374942-0. 7
- [59] Shilong Zhang, Xinjiang Wang, Jiaqi Wang, Jiangmiao Pang, Chengqi Lyu, Wenwei Zhang, Ping Luo, and Kai Chen. Dense Distinct Query for End-to-End Object Detection. In *2023 IEEE/CVF Conference on Computer Vision and Pattern Recognition (CVPR)*, pages 7329–7338, June 2023. doi: 10.1109/CVPR52729.2023.00708. URL <https://ieeexplore.ieee.org/abstract/document/10203166>. ISSN: 2575-7075. 8